Lifetime measurement of the 6*s* level of rubidium

E. Gomez, F. Baumer, A. D. Lange, and G. D. Sprouse
Department of Physics and Astronomy, State University of New York at Stony Brook, Stony Brook, New York 11794-3800, USA

L. A. Orozco
Department of Physics, University of Maryland, College Park, Maryland 20742-4111, USA
(Received 21 February 2005; published 1 July 2005)

We present a lifetime measurement of the 6*s* level of rubidium. We use a time-correlated single-photon counting technique on two different samples of rubidium atoms, a vapor cell with variable rubidium density, and a sample of atoms confined and cooled in a magneto-optical trap. The $5P_{1/2}$ level serves as the resonant intermediate step for the two-step excitation to the 6*s* level. We detect the decay of the 6*s* level through the cascade fluorescence of the $5P_{3/2}$ level at 780 nm. The two samples have different systematic effects, but we obtain consistent results that averaged give a lifetime of 45.57 ± 0.17 ns.

DOI: 10.1103/PhysRevA.72.012502 PACS number(s): 32.70.Cs, 32.80.Pj, 32.10.Dk

I. INTRODUCTION

This paper presents our measurements of the lifetime of the 6*s* level in rubidium using time-correlated single-photon counting techniques in two different atomic environments: an atomic vapor cell, and a magneto-optical trap (MOT). This work complements and enhances our program of francium spectroscopy and weak-interaction physics [1]. We have previously measured lifetimes in francium and rubidium only in a MOT [2–7]. We use the same apparatus except for the source of atoms so we carefully address the different systematic effects that are unique to each one of them. The present measurements are necessary to understand systematic effects on the measurement of the equivalent level in francium, the 8*s* level [7].

Measurements of excited-state atomic lifetimes in the low-lying states of the *s* manifold enhance our understanding of the wave functions and the importance of correlation corrections in the theoretical calculations. Relativistic corrections in rubidium are smaller than in other heavier alkali metals such as cesium or francium. This particular level (6*s*) is of primary importance to the optical parity-nonconservation (PNC) measurements that look for the parity-forbidden dipole transition between the ground state and the first excited state with the same orbital angular momentum [8,9]. The comparison of measurements with theoretical predictions tests the quality of the computed wave functions. Calculation of the wave functions has now reached greater levels of sophistication [10,11] based on many-body perturbation theory (MBPT). Those calculations are particularly important in the interpretation of precision tests of discrete symmetries in atoms such as parity nonconservation [8] and time reversal (TR) [12].

The paper is structured as follows. We show the relationship between lifetimes and atomic structure in Sec. II. Section III presents the experimental method for the lifetime measurement with details on the two sources of atoms. Section IV has the data analysis for the lifetime measurement. Section V summarizes the results and compares them with previous results and theoretical predictions. Section VI contains the conclusions in the context of similar measurements in rubidium and francium.

II. LIFETIMES AND ATOMIC STRUCTURE

The lifetime of an exited atomic state depends on the initial- and final-state wave functions and the interaction that connects them. Since the electromagnetic interaction in atomic physics is well understood, radiative lifetimes give information on atomic structure.

The lifetime τ of an excited state is the inverse of the sum of the transition probabilities, $1/\tau_i$, for all possible decay routes:

$$\frac{1}{\tau} = \sum_i \frac{1}{\tau_i}. \tag{1}$$

The matrix element associated with a particular decay (i) between two states connected by an allowed dipole transition in free space is

$$\frac{1}{\tau_i} = \frac{4}{3}\frac{\omega^3}{c^2}\alpha\frac{|\langle J\|r\|J'\rangle|^2}{2J'+1}, \tag{2}$$

where ω is the transition energy divided by $\hbar$, c is the speed of light, α is the fine-structure constant, J' and J are, respectively, the initial- and final-state angular momenta, and $|\langle J\|r\|J'\rangle|$ is the reduced matrix element.

A calculation of the reduced matrix element requires the precise knowledge of the electronic wave functions involved. The presence of the radial operator makes the matrix element more sensitive to contributions of the wave functions at large distances from the nucleus.

III. EXPERIMENTAL METHOD

We use time-correlated single-photon counting [13] to obtain the lifetime of the 6*s* level in rubidium in a vapor cell and in a MOT. This two-step transition method is well established both for vapor cells [14] and MOTs [5,6] in alkali metals.

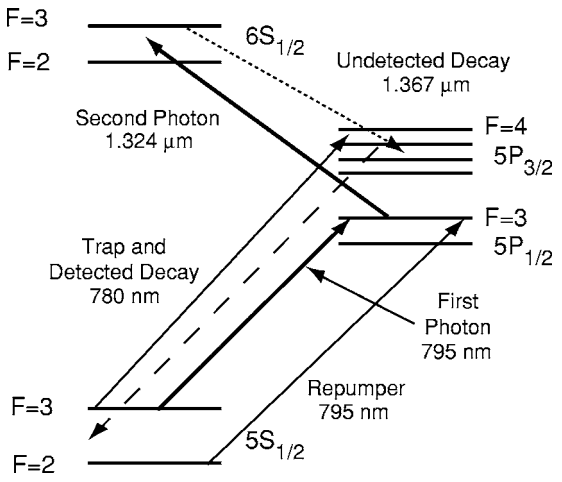

FIG. 1. Energy levels of ^{85}Rb. The figure shows the two-step excitation (solid thick lines), the fluorescence detection used in the lifetime measurement (dashed line), and the undetected fluorescence (dotted line). The trap and repumper beams (solid thin lines) are only used for the measurement in the MOT.

Figure 1 shows the energy levels of ^{85}Rb ($I=5/2$) relevant to the lifetime measurement. We excite the $6s$ level in a two-step resonant process. The first-step laser at 795 nm populates the $5P_{1/2}$ $F=3$ level and the second-step laser at 1324 nm excites the $5P_{1/2} \rightarrow 6S_{1/2}$ transition.

After we turn off the excitation lasers, the atom returns back to the ground level using two different decay channels. First, by emitting a 1324 nm photon it decays back to the $5P_{1/2}$ state and fluoresces 795 nm light to return to the $5s$ ground level. This decay path is not used for the $6s$ level lifetime measurement. The second possible decay channel is the $6s \rightarrow 5P_{3/2}$ transition followed by the decay to the $5s$ ground level. The 1367 nm fluorescence from the first step of this decay is unobserved, but we detect 780 nm light from the second part of the decay. Since the lifetime of the $5P_{3/2}$ state is well known [2,15–17], it is possible to extract the $6s$ level lifetime indirectly from the fluorescence distribution of the second step of the cascading decay.

We use a high-efficiency MOT to capture a sample of rubidium atoms at a temperature lower than 300 μK. The MOT is in line with the Stony Brook superconducting linear accelerator (LINAC) and is optimized to trap francium [18]. We load the MOT from a rubidium vapor produced by a dispenser in a glass cell coated with a dry film to reduce sticking to the walls. The MOT consists of three pairs of retroreflected beams, each with 15 mW/cm^2 intensity, 3 cm diameter ($1/e$ intensity), and red detuned 19 MHz from the atomic resonance. A pair of coils generates a magnetic field gradient of 9 G/cm. The trap contains 10^4 atoms with a diameter of 0.5 mm and a typical lifetime between 5 and 10 s.

We perform the lifetime measurement also in a vapor cell. The cell is under vacuum (approximately 10^{-5} Pa) and a dispenser provides the rubidium for the measurement. The cell is uncoated and we use no buffer gas. We keep the rubidium density low to avoid collisional quenching and radiation trapping effects. The typical mean free path of the atoms in the cell is more than 30 m. We can apply a uniform magnetic field to the cell, in contrast to the permanent magnetic field gradient in the MOT.

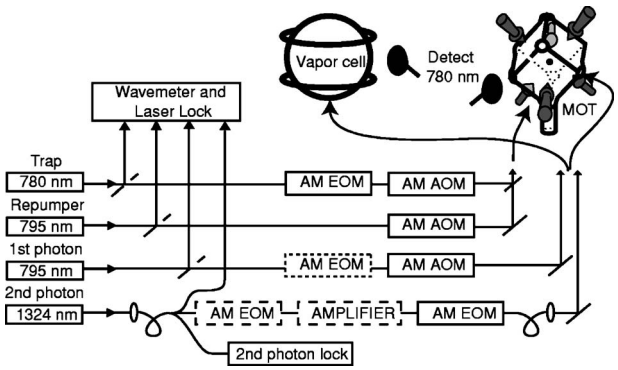

FIG. 2. Experimental setup. The trap and repumper beams are not used for the vapor cell measurement. The dotted (dashed) boxes are not used for the MOT (vapor) experiment. AM EOM is an amplitude-modulated electro-optic modulator, and AM AOM an amplitude-modulated acousto-optic modulator.

A. Laser systems

Figure 2 shows the experimental setup. We use a Coherent 899-21 titanium-sapphire (Ti:sapph) laser at 780 nm between the $5s$ $F=3$ and the $5P_{3/2}$ $F=4$ levels to trap and cool the atoms. A Coherent 899-21 Ti:sapph laser at 795 nm between the $5s$ $F=2$ and the $5P_{1/2}$ $F=3$ levels repumps any atom that falls out of the cycling transition. The trap and repumper beams are not necessary for the vapor cell measurement. We excite the atoms to the $6s$ level via a two-step transition. A Coherent 899-01 laser (or a Coherent 899-21 laser for the vapor cell) at 795 nm between the $5s$ $F=3$ and the $5P_{1/2}$ $F=3$ levels makes the first step to the $5P_{1/2}$ level and an EOSI 2010 diode laser at 1.324 μm completes the transition to the $6s$ level.

A Burleigh WA-1500 wave meter monitors the wavelength of all the lasers to about ± 0.001 cm^{-1}. We lock the trap, repumper, and first-step lasers with a transfer lock [19]. We use a different method to lock the second-step laser on the vapor cell and on the MOT measurements as described below. Figure 3 shows both locking methods for the second-step laser.

Second-step laser lock for the MOT. We transfer the stability of the helium-neon laser (Melles-Griot He-Ne 05-STP-901) used on the lock of the other lasers [19] to lock a Michelson interferometer with a 200 MHz free spectral range. The 1324 nm light propagates collinearly with the He-Ne light inside the interferometer. We detect the output of the locked interferometer at 1324 nm and use that signal to lock the second-step laser to a side of the fringe, which allows us to set it on the atomic resonance by an offset adjustment. We achieve a drift smaller than 5 MHz per hour.

Second-step laser lock for the vapor cell. We use two-step modulation transfer spectroscopy to lock the second step laser. We split the first-step laser at 795 nm into two beams and send both of them through a separate rubidium glass cell. The room-temperature vapor cell is uncoated and the beam propagates approximately 7 cm inside the cell, which leads

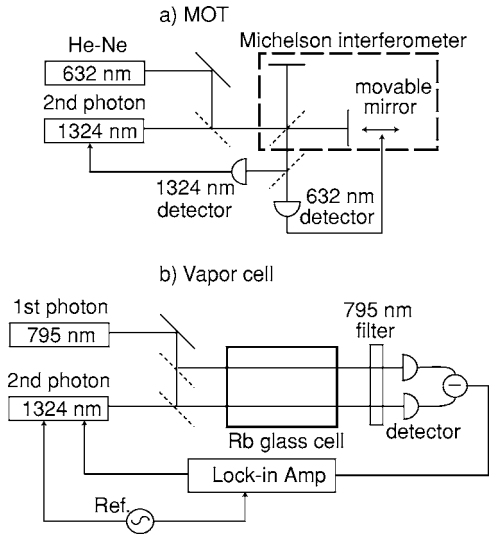

FIG. 3. Block diagram for the 1324 nm second-step laser locking system for the measurement (a) with the MOT and (b) with the vapor cell.

to a typical absorption of about 15%. We collinearly apply the 1.324 μm second-step laser to one of the beams to excite the second transition. If the laser is resonant to the two-step transition it results in less absorption of the 795 nm light. Two beams and balanced detection allow common mode noise rejection to increase the signal-to-noise ratio. We use the internal piezoelectric crystal of the 1.324 μm diode laser to dither its frequency at 1.3 kHz and perform lock-in detection of the 795 nm light transmission through the cell. We feed back the resulting error signal to the second-step laser to lock it with comparable performance to that of the Michelson lock.

We send and retroreflect 1.5 mW of the first-step laser power to the trap region. We focus it to a spot size approximately equal to the trap size. The second-step laser travels at a small angle with respect to the first-step laser and we also focus it to match the trap size with a power of 1 mW. For the vapor cell measurement the excitation beams propagate collinearly inside the glass cell. We send 100 μW of power at 795 nm and 0.4 mW of power at 1.324 μm and focus it to a spot size of about 0.6 mm.

B. Timing

Figure 4 displays the timing sequence for the excitation and decay cycle. We apply the two-step excitation 500 ns after the trap laser turnoff for a duration of 100 ns. We turn off the repumper at the same time as the two-step lasers to look for the fluorescence decay of the atoms. The counting electronics are sensitive for 500 ns to record the excitation and decay signal. The cycle repetition rate is 100 kHz. The trap and repumper pulses are not necessary for the vapor cell measurement.

Modulation for the MOT. We turn the trap laser on and off with an electro-optic modulator (EOM) (Gsänger LM0202) and an acousto-optic modulator (AOM) (Crystal Technology 3200-144) as shown in Fig. 2. The EOM gives a fast turnoff

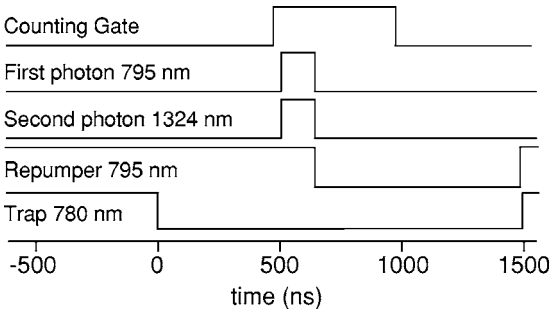

FIG. 4. Timing diagram for the 6*s* level excitation and decay cycle. The cycle repetition rate is 100 kHz. There is no trap nor repumper for the vapor cell measurement.

and the AOM improves the long-term on-off ratio. The combination of the two gives an extinction ratio of better than 1600:1 after 500 ns. We modulate the repumper and first-step laser with an AOM (Crystal Technology 3200-144) with an on-off ratio of 109:1 and 26:1, respectively, after 30 ns. We couple the 1324 nm light into a single-mode optical fiber. We use a combination of a 10 gigabits/s lithium niobate electro-optic fiber modulator (Lucent Technologies 2623N) followed by a fiber amplifier (InPhenix IPSAD1301) and a second identical fiber modulator to turn the laser on and off. The combination of the three elements gives an on-off ratio better than 1000:1 after 20 ns.

Modulation for the vapor cell. For the vapor cell measurement we do not need the trap and repumper beams and we install the EOM on the first-step laser path instead. In this case we achieve an extinction ratio of better than 100:1 in 30 ns. We reduce any radio frequency (rf) emission generated by the fast turnoff of the EOM by placing it in a separate room inside a metal cage. We use only the last fiber modulator for the 1324 nm laser and we achieve an on-off ratio of 110:1 after 20 ns. Figure 2 shows a schematic diagram of the modulation of all the lasers.

C. Imaging system

A 1:1 imaging system ($f/3.9$) collects the MOT fluorescence photons onto a charge-coupled device camera (Roper Scientific, MicroMax 1300YHS-DIF). We monitor the trap with the use of an interference filter at 780 nm in front of the camera. A beam splitter in the imaging system sends 50% of the light onto a photomultiplier tube (PMT) (Hamamatsu R636). An interference filter at 780 nm in front of the PMT reduces the background light other than fluorescence from the cascade through the $5P_{3/2}$ level decay back to the ground state $5S_{1/2}$.

The 1:1 ($f/2.4$) imaging system for the vapor cell is perpendicular to the excitation beams and collects the fluorescence from the decaying atoms to a PMT (Hamamatsu R636) with a 780 nm interference filter in front of it.

D. Detection electronics

Figure 5 shows the electronic processing of the detected fluorescence. When the PMT detects a photon, it generates a variable-amplitude electronic pulse. We first amplify the sig-

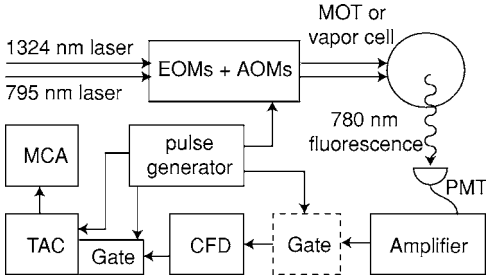

FIG. 5. Block diagram of the processing electronics. The dashed gate is not used for the vapor cell experiment. PMT, photomultiplier tube, CFD, constant fraction discriminator, TAC, time-to-amplitude converter, and MCA, multichannel analyzer.

nal with an Ortec AN106/N amplifier, send it to a linear gate (EG&G LG101/N, not used for the vapor cell measurement), and then to an Ortec 934 constant, fraction discriminator (CFD). The output of the CFD goes to a gated time-to-amplitude converter (TAC) (Ortec 467). The gating is done directly on the TAC for the MOT measurement and with an external gate (Ortec LG101/N) for the vapor cell measurement. The photon pulse starts the TAC and we stop it with an electronically generated pulse that has a fixed time delay with respect to the excitation laser pulse. Starting the TAC with a fluorescence photon eliminates the accumulation of counts from cycles with no detected photons. We use a multichannel analyzer (MCA) (EG&G Trump-8k) to produce a histogram of the events showing directly the exponential decay. A Berkeley Nucleonics Corporation BNC 8010 pulse generator is the master clock with slaved pulse and signal generators to provide the timing sequence for the measurement.

IV. DATA ANALYSIS

We extract the atomic radiative lifetime from the measured fluorescence decay. We take sets of data for about 600 s, that are individually processed, added together, and fitted. The 6*s* level decays through the 5*p* states to the 5*s* level as shown in Fig. 1 and we detect the indirect decay through the $5P_{3/2}$ state. The fitting function is a sum of two exponentials, a background and a sloping background coming from the trap laser turnoff:

$$S_{6s} = A_{6s}\exp\left(-\frac{t}{\tau_{6s}}\right) + A_{5p}\exp\left(-\frac{t}{\tau_{5p}}\right) + A_B + A_S t, \quad (3)$$

where τ_{5p} is the known lifetime of the $5P_{3/2}$ state and τ_{6s} the lifetime we want to extract, A_{6s} and A_{5p} are the coefficients of the exponentials, and A_B and A_S characterize the background. $A_S=0$ for the vapor cell measurement since there is no trap laser. Equation (4) reduces to a single exponential if one waits long enough after the turnoff to take data [20]. We instead maximize the statistics by including both exponentials in our analysis.

The first part in the data analysis requires a pile-up correction that accounts for the preferential counting of early events [13]. If N_i is the number of counts in the MCA channel i, and N_E is the total number of excitation cycles, then N'_i

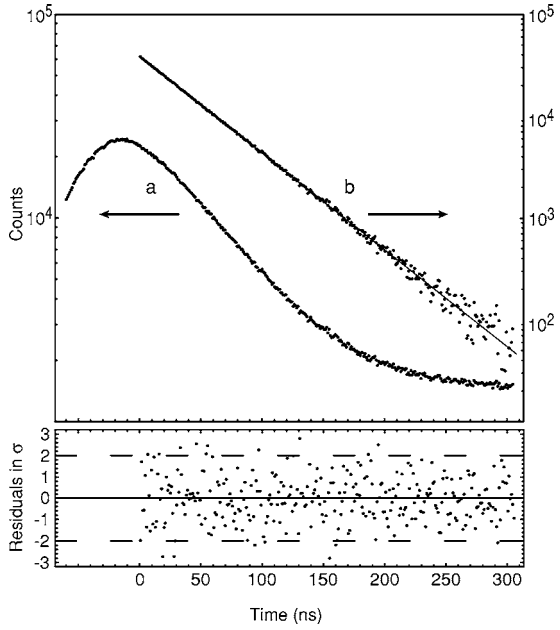

FIG. 6. Decay curve of the 6*s* level through the $5P_{3/2}$ state in the vapor cell with fit and residuals. The upper plot shows the raw arrival time histogram data for the vapor cell measurement (curve *a*) and the data after the pile-up correction and substraction of background and the $5P_{3/2}$ decay (curve *b*). The lower plot shows the normalized residuals. $\chi^2_\nu=0.98$.

is the corrected number of counts in channel i given by

$$N'_i = \frac{N_i}{1-(1/N_E)\sum_{j=1}^{i-1} N_j}. \quad (4)$$

As low count rates keep this correction small, we collect data with a small number of fluorescence photons. We typically count one photon every 100 cycles, which corresponds to a correction in the fitted lifetime by 0.1%.

We perform a nonlinear least squares fit using Microcal™ ORIGIN™ Version 5.0 to find the fitting parameters that produce the smallest χ^2. We have tested the software independently to validate and understand its results. Figure 6 shows an example of the fitting procedure. We start the fit 20 ns (25 ns for the vapor cell measurement) after both excitation lasers are off. The fitting function describes the data well, and the reduced χ^2_ν of this particular decay is 0.98. The average χ^2_ν for the MOT data is 1.05 ± 0.06 and for the vapor cell 1.09 ± 0.08. A discrete Fourier transform of the residuals shows no structure.

The MOT and vapor cell measurements have some characteristics that are intrinsically different between them. The MOT cools the atoms to a very low temperature, while the atoms in the vapor cell have temperatures corresponding to Doppler shifts significantly larger than the natural linewidth of the transitions of interest. The MOT has a magnetic field gradient always present which can be removed for the vapor cell. These differences generate systematic effects that are intrinsic to each system. We classify the systematic effects into two groups, common effects to both the MOT and the

vapor cell measurement and distinct effects that appear in a different way in the two systems.

A. Common systematic effects

1. Truncation uncertainty

The truncation uncertainty takes into account the variation of the fitted lifetime depending on the start and end points of the fit. We find no statistically significant change in the obtained lifetime when we change either the initial or final point of the fit.

2. Time calibration

We calibrate the scale on the MCA by sending a series of artificial start and stop pulses with known delay directly to the TAC either from one of the DG535 pulse generators or from two DG535 pulse generators triggered by a frequency synthesizer (Rockland 5600). The linear fit to the resulting data contributes ± 0.01%% to the lifetime uncertainty and it is consistent using either source of calibration pulses.

3. TAC and MCA response nonuniformity

A nonuniformity in the TAC or MCA results in different bins of the MCA having different response sensitivities that alter the obtained lifetime. We measure the height uniformity of the TAC-MCA system by triggering the PMT with random photons from a white light source. The nonuniformity of the TAC and MCA contributes 0.11% (0.02% for the vapor cell measurement) to the uncertainty of the lifetime. The need for additional electronic gates in the MOT measurement increases the nonuniformity in the electronics response. The response changes slightly between days. It shows up in the data as an additional noise contribution that is responsible for the deviation of the χ_ν^2 from 1. The effect is already included in this uncertainty contribution.

4. Imperfect laser turnoff

An imperfect turnoff of the excitation lasers influences the observed decay signal. If the second-step laser is not completely turned off during the decay, atoms that decay to the $5P_{1/2}$ state can be reexcited to the $6s$ level. We test the turnoff by comparing the lifetime obtained when we leave the first-step laser continuously on or off during the decay. We establish a limit of 0.07% for the effect of the imperfect turnoff of the second-step laser in the MOT measurement.

We use two modulators for the second-step laser on the MOT measurement to achieve a large on-off ratio. The vapor cell measurement uses only one modulator and we apply a correction to the obtained lifetime.

The Appendix presents the model used to calculate the effect of an imperfect turnoff on the lifetime. We solve the rate equations and compare the result obtained with a perfect turnoff to the experimental one. We find a correction to the lifetime of −0.11 ns and a sensitivity analysis of the parameters of the model gives an uncertainty contribution of ± 0.1%.

5. Initial-state conditions

The lifetime should be independent of the populations of the different levels at the beginning of the decay. We can change the initial-state conditions by changing the power of the first- or second-step laser pulses, or their duration. We calculate the linear correlation coefficient and its integral probability to study the correlation between the obtained lifetime and the external variable. The larger the integral probability is, the less likely it is that a correlation exists [21].

We vary the power of the first- and second-step lasers by more than an order of magnitude. In the vapor cell measurement we also changed the excitation pulse duration between 50 ns and 200 ns. In all the above cases we found results consistent with no correlation.

B. Distinct systematic effects

1. Radiation trapping

The fluorescence photons from atoms decaying from the $5P_{3/2}$ state to the $5s$ ground level can excite other atoms that are in the ground state and take them to the $5P_{3/2}$ level, the so-called radiation trapping [22,23]. Traps are very convenient systems to make measurements because the atoms are collected into a small region of space. The effect of radiation trapping is small in a low-density trap because the distance d corresponds to the diameter of the trap, which is rather small. Vapor cells, on the other hand, may have a large density, but Doppler shifts reduce the effective number of atoms that could reabsorb the fluorescence.

The probability of a photon being absorbed by an atom can be deduced from Beer's law

$$I(d) = I_0 \exp(-\alpha d), \tag{5}$$

where I_0 is the initial intensity, $I(d)$ is the intensity after traversing the distance d, and $\alpha = \sigma n$ represents the absorption coefficient, with n the density of the atomic vapor and $\sigma = 3\lambda^2 f/2\pi$ the absorption cross section. $f = 0.69$ is the oscillator strength of the corresponding transition. For small absorption the probability P of a photon being absorbed by the atoms is $P = \sigma n d$.

The rate equation for the $5P_{3/2}$ level in the presence of radiation trapping after the lasers turn off is given to first order by

$$\frac{dN_{5p}}{dt} = B_{5p}\frac{N_{6s}}{\tau_{6s}} - \frac{N_{5p}}{\tau_{5p}} + \frac{N_{5p}}{\tau_{5p}}P, \tag{6}$$

with N_{5p} and N_{6s} the number of atoms in the $5P_{3/2}$ and $6s$ levels and B_{5p} the branching ratio from the $6s$ level to the $5P_{3/2}$. In this approximation the change in the lifetime of the $5P_{3/2}$ level is directly proportional to P. As our fitting process assumes a fixed $5P_{3/2}$ state lifetime, the change due to radiation trapping propagates linearly to the measured $6s$ level lifetime.

We vary the density of rubidium atoms to look for variations in the lifetime. We change the density by changing the number of atoms in the MOT or by compressing the trap with an increase the magnetic field gradient. We establish a limit of 0.01% for the effect of radiation trapping on the lifetime.

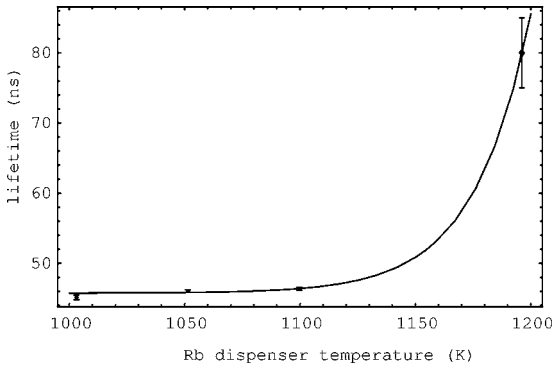

FIG. 7. Temperature dependence of the measured 6*s* level lifetime together with a fit.

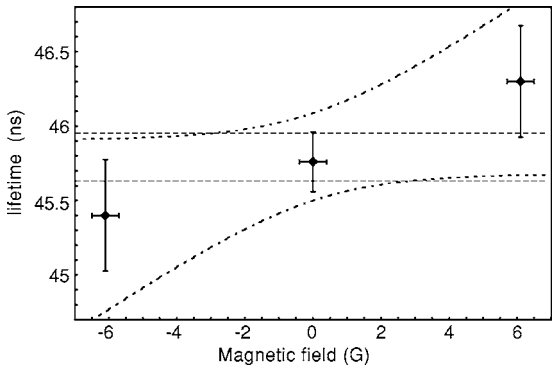

FIG. 8. Magnetic field dependence of measured lifetime in the vapor cell. The plot contains the 1σ region for the linear fit to the data (dotted line) and the error on the average assuming no linear dependence (dashed line).

A rubidium dispenser (SAES) provides the atoms in the vapor cell measurement. A zirconium alloy matrix releases rubidium atoms when it is heated by a dc current. The desorption follows an Arrhenius process that requires a certain activation energy E_a. The atomic density in the cell follows the relation

$$n(T) \propto \exp\left(\frac{k_B T}{E_a}\right), \tag{7}$$

where k_B is the Boltzmann constant and T the temperature in kelvins. Measurements of the pressure on the cell confirm this relationship.

We compare the lifetime obtained at different dispenser temperatures and extrapolate the observed dependency to zero temperature to obtain the correction to the lifetime. The fitting function for the temperature dependence of the observed lifetime is

$$\tau(T) = \tau_0 + A \exp(T/B), \tag{8}$$

where A, B, and the corrected lifetime τ_0 are fitting constants. Figure 7 shows the measured data and the obtained fit. The correction of the 6*s* level lifetime due to radiation trapping amounts -0.28 ± 0.17 ns. The error in the correction is very large (60%). It comes from the fit as we extrapolate with a limited number of data points that depend exponentially on the temperature. Any future measurements using a vapor cell will require a more detailed study of this effect to reduce the error contribution. The uncertainty contribution to the lifetime (0.38%) is the dominant uncertainty in the vapor cell measurement.

2. Magnetic field

The presence of a magnetic field can influence the measured lifetime through quantum beats between Zeeman sublevels. In ideal conditions the atoms in a MOT sit at the zero of the magnetic field gradient, but in reality an imbalance of the power of the retroreflected beams may displace the trap from this ideal position. The use of a cascade decay reduces the appearance of quantum beats [14,24].

We quantify the magnetic sensitivity of the lifetime measurement in two ways. First we perform the measurement at different magnetic field gradients. We do not observe a correlation with the magnetic field gradient and we establish a limit on the effect of the magnetic field on the lifetime of 0.17%. This limit is consistent with measurements done in the vapor cell. Alternatively, we keep the magnetic field environment fixed and we displace the trap by creating an imbalance on the laser beams that interact with it. We can imbalance the trap beams by inserting a piece of glass in front of one of the retroreflection mirrors, and repeating the same for all three axes. Changing the power of the first-step laser beam also displaces the trap. The change in the obtained lifetime in all cases is consistent with statistical fluctuations.

The measurement in the vapor cell does not require a magnetic field gradient. We generate a homogeneous magnetic field with two coils arranged close to a Helmholtz configuration with its axes in the same direction as the excitation laser beams. The magnetic field homogeneity in the excitation region is ± 0.35%.

Figure 8 shows the measured 6*s* level lifetime in the vapor cell as a function of the external uniform magnetic field. We can control the magnetic field to ±0.2 G due to the earth magnetic field and other magnetic sources. Although the eye sees a dependence, the correlation coefficient for the three data points, considering their error bars, is consistent with no correlation. The dotted line shows the 68% confidence band (1σ) on the linear fit for a t distribution with one degree of freedom. The dashed line gives the error on the average assuming no linear dependence. The figure shows that the two regions are consistent with each other. We limit the contribution to the uncertainty due to magnetic fields to ±0.07% using the linear fit to the data.

3. Collisional quenching

Inelastic collisions can modify the lifetime of an excited state. The velocity of atoms in the MOT (vapor cell) is smaller than 0.1 m/s (250 m/s). The mean free path of the atoms in the MOT (vapor cell) is about 10^4 m (10 m); the effect of collisions is negligible for both samples.

4. Time of flight

A moving atom can escape the imaging area before it decays. The effect is more evident in the vapor cell where the

TABLE I. Experimental results for the rubidium $5P_{3/2}$ lifetime.

Reference	Lifetime (ns)
Simsarian *et al.* [2]	26.20(9)
Volz *et al.* [15]	26.24(4)
Gutterres *et al.* [17]	26.25(8)
Heinzen *et al.* [16]	26.23(6)

atoms have larger speeds. The MOT (vapor cell) imaging area has a 1 mm (5.5 mm) diameter aperture. It takes an atom on average 10^5 (200) lifetimes to leave the MOT (vapor cell) imaging area. A Monte Carlo simulation shows no statistically significant change in the lifetime for the vapor cell measurement.

5. Background slope

The detected light at 780 nm comes from the cascade decay from the 6s level, but also from scattered light from the trap laser. We turn off the trap laser 500 ns before the two-step excitation, but the remanent of the trap laser light appear in the signal as an slope in the background. Fits to files with and without decaying atoms give consistent values for the background slope. We compare the lifetime obtained when we leave the background slope as a free parameter or when we fix it to the value obtained without two-step excitation and obtain an uncertainty contribution of ± 0.22%. This contribution does not appear in the vapor cell measurement since there is no trap laser.

6. PMT response

We look for saturation effects in the PMT due to the trap light by comparing the PMT response to that of a fast photodiode which is not subject to saturation. We replaced the two-step excitation by a light pulse at 780 nm. Comparison of the detected pulse in the PMT and in the fast photodiode gives a maximum contribution to the uncertainty of ± 0.21%. This effect is not present in the vapor cell measurement.

V. RESULTS AND COMPARISON WITH THEORY

The lifetime of the 6s level depends on the value of the lifetime of the $5P_{3/2}$ state. The uncertainty of the $5P_{3/2}$ state lifetime propagates to the uncertainty of the 6s level lifetime. Using Bayesian statistics the contribution to the uncertainty ($\sigma_{B_{6s}}$) due to the $5P_{3/2}$ level is given by [5]

$$\sigma_{B_{6s}} = \frac{d\tau_{6s}(\tau')}{d\tau'}\sigma_{5p}. \tag{9}$$

We assume different values τ' for the lifetime of $\tau_{5P_{3/2}}$ and include them in the fitting function [Eq. (4)] to obtain the dependence of $\tau_{6s}(\tau')$.

The $5P_{3/2}$ level lifetime has been measured previously by several groups (see Table I). We take the weighted average of all the measurements. We add the systematic contributions of the respective errors in quadrature and calculate the total statistical contribution according to $\sigma^2_{\text{stat}}=(\Sigma 1/\sigma_i^2)^{-1}$ where σ_i is the statistical uncertainty of a single result. The $5P_{3/2}$-state lifetime of 26.23(9) ns gives a Bayesian error for the 6s level lifetime of 0.17% (0.11% for the vapor cell).

TABLE II. Error budget and corrections for the 6s level lifetime measurement in the vapor cell.

	Correction	Percent error
Time calibration		±0.01
Bayesian error		±0.11
TAC and MCA nonuniformity		±0.02
Imperfect laser turnoff	−0.11 ns	±0.10
Radiation trapping	−0.28 ns	±0.38
Magnetic field		±0.07
Statistical error		±0.24
Total		±0.48

TABLE III. Error budget for the 6s level lifetime measurement in the MOT.

	Percent error
Time calibration	±0.01
TAC and MCA nonuniformity	±0.11
Radiation trapping	±0.01
Imperfect laser turnoff	±0.07
Magnetic field	±0.17
Background slope	±0.22
PMT response	±0.21
Bayesian error	±0.17
Statistical error	±0.38
Total	±0.56

Tables II and III contain the error budget and the corrections for the 6s level lifetime measurement in the vapor cell and in the MOT. The error is dominated by the statistical uncertainty in the MOT and by radiation trapping in the vapor cell. The vapor cell corrections change the result by −0.9%. We obtain a lifetime of 45.64±0.22 ns in the vapor cell and 45.48± 0.25 ns in the MOT for the 6s level lifetime. The two results are consistent with each other and the average gives 45.57± 0.17 ns.

Figure 9 compares the obtained 6s level lifetime with (a) a previous measurement by Marek *et al.* [25], (b) and (c) *ab initio* many-body perturbation theory calculations by Safronova *et al.* [26] and Johnson *et al.* [27], and (d) a semiempirical prediction using a one-electron effective-potential model by Theodosiou *et al.* [28].

VI. CONCLUSIONS

The consistency of lifetime results using two different sources of atoms demonstrates the understanding achieved in the systematic effects present in this technique. The MOT source has advantages in density, temperature, and radiation trapping compared to a room-temperature cell; however, the intrinsic magnetic gradient has been a source of concern.

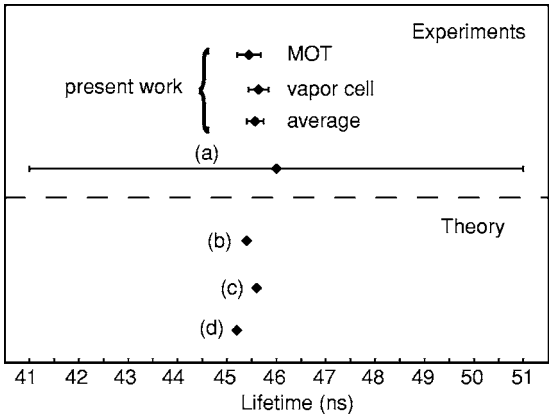

FIG. 9. Comparison of the present measurement of the 6*s* level lifetime (45.57±0.17 ns) with previous experimental results (a) by Marek *et al.* [25] and theoretical predictions by (b) Safronova *et al.* [26] (c) Johnson *et al.* [27], and (d) Theodosiou *et al.* [28].

This work sets a lower limit on the influence of these effects by doing the measurement with two atomic sources. Statistics limit the MOT results, while the radiation trapping is the limiting factor in the glass cell. This measurement improves previous determinations by a factor of 30.

Our measurement of the lifetime of the first excited state in the *s* manifold of rubidium has reached a precision of 0.3%, which permits a very careful tests of the calculated matrix elements that contribute to the lifetime of the 6*s* state. These *ab initio* MBPT calculations represent the state of the art in atomic structure calculations and require a very thorough understanding of the electron correlations and many other subtle effects that add and subtract in the expansions. The same techniques applied for rubidium are used in cesium, and the agreement between experiment and theory enhances the confidence in the established calculation techniques to provide the necessary information such as matrix elements for the extraction of weak-interaction parameters from the PNC measurements in cesium and in future measurement in other alkali-metal atoms.

ACKNOWLEDGMENTS

This work was supported by NSF. E.G. acknowledges support from CONACYT and the authors thank the personnel at the Nuclear Structure Laboratory at Stony Brook for their support and J. Gripp, J. E. Simsarian, and Bill Minford for equipment loans for this work.

APPENDIX

We calculate the effect of the imperfect laser turnoff by including it in the rate equations as a small perturbation and compare the result to the unperturbed solution. For simplicity we rename the $6s, 5P_{3/2}, 5P_{1/2}$, and $5s$ levels as 1, 2, 3, and 4, respectively. The rate equations with the two-step excitation on are

$$\dot{N}_1 = -\frac{N_1}{\tau_1} + e_1 N_3,$$

$$\dot{N}_2 = -\frac{N_2}{\tau_2} + B_2 \frac{N_1}{\tau_1},$$

$$\dot{N}_3 = -\frac{N_3}{\tau_3} + e_3 N_4 + B_3 \frac{N_1}{\tau_1} - e_1 N_3, \tag{A1}$$

where N_i represents the number of atoms in state i with $N_1 + N_2 + N_3 + N_4 = N$ the total number of atoms, τ_i is the lifetime of state i, e_i stands for the excitation to state i, and B_i is the branching ratio from state 1 to state i.

We take the steady-state solution of Eq. (A1) as the initial state for the decay. The solution of Eq. (A1) with $e_1 = e_3 = 0$ corresponds to the case of a perfect on-off ratio.

To calculate the perturbation introduced by the imperfect turnoff we use the unperturbed solution for $N_3(t)$ on the other two equations in the following way:

$$\dot{N}_1 = -\frac{N_1}{\tau_1} + f(t) e_1 N_3,$$

$$\dot{N}_2 = -\frac{N_2}{\tau_2} + B_2 \frac{N_1}{\tau_1}, \tag{A2}$$

with $f(t)$ the second-step laser turnoff, which is well represented by a Gaussian function ($\Delta t \approx 5$ ns) plus a constant level,

$$f(t) = (1 - a)\exp\left(\frac{t}{\Delta t}\right)^2 + a, \tag{A3}$$

where a is the on-off ratio.

We use the analytic solution of Eq. (A2) for $N_2(t)$ to generate a decay sample that we process in the same way as real data to obtain a lifetime for the 6*s* level.

We include the following parameters in the model. For the lifetimes of the $5p$ levels we use the results [2,15–17] (as in Table I) and for the branching ratios B_i we use the theoretical values calculated by Safronova *et al.* [26]. We take $e_3 = 1/\tau_3$ and to obtain e_1 we compare the observed number of counts when the excitation reaches steady state to $N_2(0)$ in the model.

The most likely parameter configuration consistent with our experimental setup gives a lifetime correction of −0.11 ns. We perform a sensitivity analysis for the model parameters to obtain an uncertainty in the lifetime of ± 0.1%.

[1] L. A. Orozco, in Trapped Particles and Fundamental Physics, edited by S. N. Atutov, R. Calabrese, and L. Moi, *Proceedings of the Les Houches Summer School of Theoretical Physics, 2000* (Kluwer Academic Publishers, Amsterdam, 2002).
[2] J. E. Simsarian, L. A. Orozco, G. D. Sprouse, and W. Z. Zhao, Phys. Rev. A **57**, 2448 (1998).
[3] J. M. Grossman, R. P. Fliller III, L. A. Orozco, M. R. Pearson, and G. D. Sprouse, Phys. Rev. A **62**, 062502 (2000).
[4] S. Aubin, E. Gomez, L. A. Orozco, and G. D. Sprouse, Opt. Lett. **28**, 2055 (2003).
[5] S. Aubin, E. Gomez, L. A. Orozco, and G. D. Sprouse, Phys. Rev. A **70**, 042504 (2004).
[6] E. Gomez, S. Aubin, L. A. Orozco, and G. D. Sprouse, J. Opt. Soc. Am. B **21**, 2058 (2004).
[7] E. Gomez, L. A. Orozco, A. P. Galvan, and G. D. Sprouse, e-print physics/0412073, Phys. Rev. A (to be published).
[8] C. S. Wood, S. C. Bennett, J. L. Roberts, D. Cho, and C. E. Wieman, Can. J. Phys. **77**, 7 (1999).
[9] J. Guéna, D. Chauvat, P. Jacquier, E. Jahier, M. Lintz, S. Sanguinetti, A. Wasan, M. A. Bouchiat, A. V. Papoyan, and D. Sarkisyan, Phys. Rev. Lett. **90**, 143001 (2003).
[10] W. R. Johnson, M. S. Safronova, and U. I. Safronova, Phys. Rev. A **67**, 062106 (2003).
[11] J. S. M. Ginges and V. V. Flambaum, Phys. Rep. **397**, 63 (2004).
[12] I. B. Khriplovich and S. K. Lamoreaux, *CP Violation without Strangeness: Electric Dipole Moments of Particles, Atoms and Molecules* (Springer-Verlag, New York, 1997).
[13] D. V. O'Connor and D. Phillips, *Time Correlated Single Photon Counting* (Academic, London, 1984).
[14] B. Hoeling, J. R. Yeh, T. Takekoshi, and R. J. Knize, Opt. Lett. **21**, 74 (1996).
[15] U. Volz and H. Schmoranzer, Phys. Scr. **65**, 48 (1996).
[16] D. J. Heinzen (private communication).
[17] R. F. Gutterres, C. Amiot, A. Fioretti, C. Gabbanini, M. Mazzoni, and O. Dulieu, Phys. Rev. A **66**, 024502 (2002).
[18] S. Aubin, E. Gomez, L. A. Orozco, and G. D. Sprouse, Rev. Sci. Instrum. **74**, 4342 (2003).
[19] W. Z. Zhao, J. E. Simsarian, L. A. Orozco, and G. D. Sprouse, Rev. Sci. Instrum. **69**, 3737 (1998).
[20] D. DiBerardino, C. E. Tanner, and A. Sieradzan, Phys. Rev. A **57**, 4204 (1998).
[21] P. R. Bevington and D. K. Robinson, *Data Reduction and Error Analysis for the Physical Sciences*, 3rd ed. (McGraw-Hill, New York, 2002).
[22] T. Holstein, Phys. Rev. **72**, 1212 (1947).
[23] M. Beeler, R. Stites, S. Kim, L. Feeney, and S. Bali, Phys. Rev. A **68**, 013411 (2003).
[24] P. Knight, Opt. Commun. **32**, 261 (1980).
[25] J. Marek and P. Munster, J. Phys. B **13**, 1731 (1980).
[26] M. S. Safronova, C. J. Williams, and C. W. Clark, Phys. Rev. A **69**, 022509 (2004).
[27] W. R. Johnson, Z. W. Liu, and J. Sapirstein, At. Data Nucl. Data Tables **64**, 279 (1996).
[28] C. E. Theodosiou, Phys. Rev. A **30**, 2881 (1984).